# Sensing and Communication in UAV Cellular Networks: Design and Optimization

Carles Diaz-Vilor, *Graduate Student Member, IEEE*, Mojtaba Ahmadi Almasi, *Member, IEEE*, Amr M. Abdelhady, *Member, IEEE*, Abdulkadir Celik, *Senior Member, IEEE*, Ahmed M. Eltawil, *Senior Member, IEEE*, and Hamid Jafarkhani, *Fellow, IEEE* 

Abstract—Recently, the use of uncrewed aerial vehicles (UAVs) in joint sensing and communication applications has received a lot of attention. However, integrating UAVs in current cellular systems presents major challenges related to trajectory optimization and interference management among others. This paper considers a multi-cell network including a UAV, which senses and forwards the sensory data from different events to the central base station. Particularly, the current manuscript covers how to design the UAV's (i) 3D trajectory, (ii) power allocation, and (iii) sensing scheduling such that (a) a set of events are sensed, (b) interference to neighboring cells is kept at bay, and (c) the amount of energy required by the UAV is minimized. The resulting nonconvex optimization problem is tackled through a combination of (i) low-complexity binary optimization, (ii) successive convex approximation, and (iii) the Lagrangian method. Simulation results over a range of various key parameters have shown the merits of our approach, which consumes 33%-200% less energy compared to different benchmarks.

Index Terms—UAV, sensing, communications, trajectory optimization, interference management, energy-efficiency, 6G

## I. INTRODUCTION

The transition towards 6G networks has started with a potential use case of combining sensing and communications under the same umbrella [1]-[3]. While static sensing and/or communication networks have been greatly studied, efficient sensing and reliable communication in dynamic networks result in new challenges not perceived by the static counterparts. To circumvent these challenges, the uncrewed aerial vehicle (UAV) technology presents an appealing framework. Indeed, because of their advantages, e.g. low production cost or easy deployment and control, the use of UAVs in wireless communication systems has attracted significant attention during the last few years. Specifically, deploying UAVs and other nodes under certain optimality criteria is an active field of research [4]–[25]. For example, authors in [9], [10], [12] regard UAVs as flying base stations with the goal of maximizing the minimum rate whereas [14], [15] exploit the relaying capabilities of the UAVs. Additionally, [23]–[25] present a variety of

C. Diaz-Vilor, M. Ahmadi Almasi, and H. Jafarkhani are with the Center for Pervasive Communications and Computing, Univ. of California, Irvine. Emails: {cdiazvil, maalmasi, hamidj} at uci.edu. Their work was supported in part by the NSF Award CNS-2209695.

A. M. Abdelhady, A. Celik, and A. Eltawil are with with the Computer Electrical, and Mathematical Science and Engineering (CEMSE) Division, King Abdullah Univ. of Science and Technology (KAUST), Kingdom of Saudi Arabia {amr.abdelhady, abdulkadir.celik, ahmed.eltawil} at kaust.edu.sa. Their work was supported in part by NEOM under grant number 4849 and KAUST.

UAV-aided data-collection networks. However, jointly tackling sensing and communications problems is novel with few works dealing with it [26]–[29].

Compared to earlier results, this manuscript covers unsolved fundamental challenges that naturally arise in joint sensing and communication networks such as the 3D UAV trajectory optimization, interference management, and sensing scheduling. One important defining aspect of these networks is data collection versus sensing. In data collection UAV networks, sensing is done on the ground and a communication link between the ground device and the UAV is needed. On the other hand, in sensing UAV networks, UAVs sense the events cooperatively whilst guaranteeing a successful sensing probability. For example, UAVs can be equipped with a variety of cameras and sensors which, after sensing an event, generate a certain amount of data that is transmitted to the base station (BS) [30]–[32].

In fact, the vast majority of the literature separates sensing from communications, especially within UAV networks given the complexity of achieving optimal deployments. Therefore, this work aims at filling this gap by focusing on the UAV-energy minimization problem with respect to (i) 3D UAV trajectory, (ii) power allocation, and (iii) sensing in multi-cell UAV-aided networks constrained to a set of sensing, communications, and mechanical technical specifications. Concretely, each cell provides service to a set of ground users (GUs). In addition, the central cell also contains a set of events that must be sensed by the UAV, that can be regarded as an aerial user which always reports to the central BS<sup>1</sup>. After sensing an event, usually represented through a probabilistic sensing model [33]–[35], the UAV generates the sensory data which is transmitted to the central BS over a certain resource block.

Unlike the existing works in the literature, we envision a time-dependent probability of sensing, i.e., longer periods flying close to an event result in higher sensing probabilities. In addition, the sensory data transmission is mainly constrained by the information causality, UAV mobility, and interference. In fact, compared to [22], [24], and similar works, the constraints that preserve the causality of the information need to be redefined. Two major differences arise: (*i*) the UAV uses the same resource block at all times without any time or frequency scheduling, and (*ii*) there is no link between the events and UAV as previously mentioned. As a consequence, the spectral

<sup>1</sup>Minor modifications would apply if handovers between the UAV and the BSs were considered.

efficiency of this system is higher although a reformulation of the causality constraint is needed. Moreover, a significant issue that is often ignored when designing UAV networks, as in [14]–[16], [19]–[22] among others, relates to interference. Particularly, it is assumed that the devices within each cell are assigned an orthogonal resource block; therefore, intracell interference is negligible, which can be easily achieved for example by orthogonal frequency division multiple access (OFDMA). However, frequency reuse among cells gives rise to inter-cell interference. Specifically, interference in aerial radio links is predominant compared to the ground counterparts given the Rician nature of air-to-ground channels [36]-[38]. Consequently, interference arising from the sensory data transmission from the UAV to the BS must be accounted for. Otherwise, correct decoding at certain GUs or BSs may fail. There are two main solutions to mitigate interference: (a) using coding or beamforming at the transmitter [39]-[42] and/or (b) perform power control at the UAV [43], [44]. In this work, to handle inter-cell interference, power control is performed at the UAV, to make it possible to carry a single antenna.

Finally, we broaden the model by considering a variable flying time. This is in contrast with most of the UAV literature, in which the flying time is fixed and predetermined. By exploiting the path discretization technique [21], we allow non-uniform time slots, which are shown to boost the UAV's energy efficiency.

The optimization problem we aim to solve is highly non-convex; hence, it is decomposed into four subproblems and is solved utilizing the block coordinate descend (BCD) approach [45]. The first subproblem deals with the logic-based sensing variables while the second jointly optimizes the UAV trajectory and time slot length by leveraging the well-known successive convex approximation method (SCA) [46], which is also applied to optimize the UAV altitudes. Finally, it is shown that the analytical expression for the UAV transmit power can be obtained through the Lagrangian method. Therefore, the main contributions of this paper can be summarized as:

- A novel scenario that integrates sensing and communications is presented in UAV-aided multi-cell cellular networks based on realistic channels, sensing models, and subject to sensing, communications, and mechanical constraints.
- The UAV energy minimization problem is studied as a function of the 3D UAV path, sensing, and transmit power which results in a mixed-integer nonlinear programming problem.
- Capitalizing on four low-complexity subproblems, suboptimal solutions minimizing the on-board UAV energy are obtained. The sensing is handled through a lowcomplexity binary optimization algorithm while the SCA technique is used to optimize the UAV's path. Finally, the optimal UAV transmit power is analytically obtained.
- The impact and tradeoffs between a variety of parameters is well established. Our results show that the proposed scheme outperforms other benchmark methods and reduces the energy consumption between 33%-200%.

The remainder of the paper is organized as follows. Sec-

tion II presents the complete system model for the UAVenabled sensing and communications network. The problem formulation and solution are studied in Sections III and IV, respectively. Numerical results are presented and discussed in Section V while concluding remarks are set forth in Section VI

*Notation:* lowercase letters, lowercase bold letters, and capital bold letters denote scalars, vectors, and matrices, respectively. A circularly symmetric complex Gaussian random variable (r.v.) is denoted by  $\mathcal{N}_{\mathbb{C}}(a,b)$ , with mean a and variance b, while  $\mathcal{U}[a,b]$  denotes a uniform r.v. on the range [a,b].

## II. SYSTEM MODEL

Consider a cellular network composed of multiple cells as shown in Fig. 1. Each cell contains one BS while the central cell also features one UAV and M events that need to be sensed with  $\mathcal{M} = \{1, \dots, M\}$  denoting the set of events of interest. Particularly, the mth event of interest is located inside the central cell<sup>2</sup> at  $\ell_m = (\boldsymbol{l}_m, 0)$  with  $\boldsymbol{l}_m \in \mathbb{R}^{2 \times 1}$  whose coordinates are known a priori via different techniques such as Global Positioning System (GPS)<sup>3</sup>. The flying/mission time is represented by T and the corresponding UAV coordinates at time t are given by  $\ell(t) = (q(t), H(t))$  where  $q(t) \in \mathbb{R}^{2 \times 1}$ represents the ground coordinates and H(t) denotes the flying altitude. The BSs are located at the center of each cell. However, provided that the UAV reports to the BS in the central cell, only the location of such BS is relevant, whose coordinates are  $\ell_B = (q_B, H_B)^4$ . For the kth GU outside the central cell, its coordinates are  $\ell_k = (w_k, 0)$ . Particularly,  $\{q_B, w_k\} \in \mathbb{R}^{2 \times 1}$  and  $H_B$  is the BS altitude, common for all of them. The optimization with respect to continuous time variables would yield to an intractable problem since the number of optimization variables is infinite. Therefore, the mission time T is discretized into N non-uniform time slots, denoted by  $\delta(n)$ , whose lengths are included in the optimization problem. Consequently,  $T=\sum\limits_{n=1}^{N}\delta(n)$  and thus the UAV's path is discretized, where the 3D coordinates at slot n are represented by  $\ell(n) = (q(n), H(n))$ . Usually, discretizing the trajectory only specifies the locations whereas discretizing the path involves both the locations and the time dimension [21]. To maintain the sampling accuracy, an appropriate value for N must be chosen by imposing the following constraint

$$||\boldsymbol{\ell}(n+1) - \boldsymbol{\ell}(n)|| \le d_{\max},\tag{1}$$

where  $d_{\rm max}$  is a proper value such that the UAV is assumed to fly at a constant velocity within each segment and the parameter variation between two successive time slots is small. In fact, when  $d_{\rm max} \to 0$ , then  $N \to \infty$  and a nearly continuous trajectory is obtained. To obtain a scalable N that satisfies (1), one can first obtain an upper bound on the flying

<sup>&</sup>lt;sup>2</sup>Our formulation and solutions apply to the general case in which the events are located at different cells.

<sup>&</sup>lt;sup>3</sup>The impact of inaccurate locations is left as future work.

<sup>&</sup>lt;sup>4</sup>Minor modifications will be needed if the central cell has to handover the UAV to another cell. If such a handover happens, the other BS location will be relevant as well.

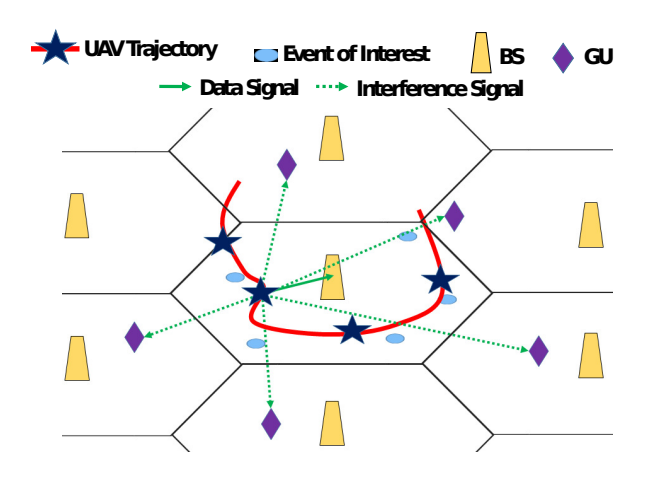


Fig. 1: A multi-cell network with UAV-aided communications and sensing.

distance, given by  $D_{\rm max}$ , and require  $(N+1)d_{\rm max}>> D_{\rm max}$ . Consequently, under the worst case scenario of the UAV flying  $D_{\rm max}$ , the sampling accuracy is still preserved. For ease of exposition, we define  $d_B(n)$  and  $d_k(n)$  as the Euclidean distance from the UAV to the central BS and User k, respectively.

#### A. Channel Model

The channel coefficient between the UAV and any of the network elements, denoted by  $g_i(n)$  for  $i \in \{B, k\}$ , follows a Rician distribution, which encompasses two elements: (a) the LoS component and (b) a Rayleigh-distributed small-scale fading component [47, Sec. 3.4.1]

$$g_{i}(n) = \sqrt{\frac{\beta_{0}}{d_{i}^{\kappa}(n)\left(K_{i}(n)+1\right)}} \left[\sqrt{K_{i}(n)}e^{j\psi_{i}(n)} + a_{i}(n)\right]$$
 for  $i \in \{B, k\},$ 

where  $\beta_0$  and  $\kappa$  are the path loss at a reference distance of 1m and the path loss exponent, respectively. The Rician factor is  $K_i(n)$ , which depends on the geometry between transmitter and receiver and environmental parameters [37]. Finally,  $\psi_i(n) \sim \mathcal{U}[0,2\pi]$  and  $a_i(n) \sim \mathcal{N}_{\mathbb{C}}(0,1)$  account for the phase rotation and the small-scale fading, respectively.

## B. Rate Calculation

The UAV can be regarded as an aerial user within the central cell. Therefore, it is assigned an orthogonal resource block, avoiding interference to the GUs within the central cell. Upon sensing an event, the UAV generates and transmits the sensory data to the BS with an instantaneous rate of

$$R(n) = \log_2\left(1 + \frac{|g_B(n)|^2 p(n)}{\sigma^2}\right),$$
 (3)

where  $\sigma^2$  denotes the noise power and p(n) is the UAV's transmit power, which must not exceed a certain value:

$$p(n) \le p_{\max},\tag{4}$$

where  $p_{\max}$  is the maximum transmit power. A common approach to manage the randomness of the rate is to consider the ergodic capacity, i.e.,  $\mathbb{E}\{R(n)\}$ . Furthermore, application of Jensen's inequality to  $\mathbb{E}\{R(n)\}$  removes the effect of the small-scale fading given that  $\mathbb{E}\{|g_B(n)|^2\} = \frac{\beta_0}{d_B^\kappa(n)}$ . As shown in [16], to keep the contribution of the LoS and NLoS channel components, the channel coefficient can be well approximated by a logistic regression. Therefore, as suggested in [16], the rate is approximated as

$$R(n) = \log_2 \left( 1 + \left( C_1 + \frac{C_2}{1 + e^{-(B_1 + B_2 u_B(n))}} \right) \frac{\beta_0 p(n)}{d_B^{\kappa}(n) \sigma^2} \right), \tag{5}$$

where  $C_1$ ,  $C_2$ ,  $B_1$ , and  $B_2$  are obtained from the logistic model and  $u_B(n)=\frac{(H(n)-H_B)}{d_B(n)}$ .

## C. Interference Management

A key enabler in wireless cellular networks is interference management. While intra-cell interference can be avoided through well-known techniques such as OFDMA, neighboring cells will reuse some of the resources<sup>5</sup>. Consequently, given the dominance of the LoS component in aerial channels, intercell interference arises at both the BSs and the GUs originated by the UAV transmissions<sup>6</sup>. Therefore, to keep interference at a bay, a joint optimization of the UAV trajectory and power is considered, in recognition that an isolated study of one aspect may be misleading because of potential bottlenecks in the other. By using the same logistic regression approximation for the channels between the UAV and GUs (or neighboring BSs), the amount of interference that GU k receives from the UAV is:

$$I_k(n) = \left(C_1 + \frac{C_2}{1 + e^{-(B_1 + B_2 u_k(n))}}\right) \frac{\beta_0 p(n)}{d_k^{\kappa}(n)}.$$
 (6)

Therefore, the following interference-related constraint must be met for each of the GUs:

$$I_k(n) \le I_{\text{th}},$$
 (7)

where  $I_{\rm th}$  is the maximum level of interference each GU can tolerate without compromising the decoding.

# D. Energy Consumption Model

We consider a realistic energy consumption model for the UAV comprised of (i) flying power  $p_f(n, \ell(n), \delta(n))$ , (ii) sensing power  $p_s$ , and (iii) communication power p(n) [48]–[50]. Following [21], for rotatory-wing UAVs, the total UAV energy, spent over the N time slots, is

$$E = \sum_{n=1}^{N} \delta(n) \left( p_f(n, \ell(n), \delta(n)) + \sum_{m=1}^{M} \alpha_m(n) p_s + p(n) \right),$$
(8)

<sup>5</sup>A reuse factor of one is assumed while the same framework and solutions apply if other sectorization and reuse factors are assumed. The sectorization or reuse factor will only affect the number of interference-related constraints not their nature.

<sup>6</sup>In practice, neighboring BSs can fully cancel the UAV's interference through beamforming techniques. However, if there is any remaining interference at neighboring BSs, an interference constraint, similar to those of GUs, can be added

where  $\alpha_m(n)$  is a logic binary variable defined as

$$\alpha_m(n) = \begin{cases} 1 & \text{if event } m \text{ is sensed at time } n \\ 0 & \text{otherwise} \end{cases} . \tag{9}$$

Based on [21], [51],  $p_f(n, \ell(n), \delta(n))$  is a function of the UAV locations and the time slots as follows

$$p_f(n, \ell(n), \delta(n)) = P_0 \left( 1 + \frac{3v(n)^2}{U_{tip}^2} \right) +$$

$$P_i \left( \sqrt{1 + \frac{v(n)^4}{4v_0^4}} - \frac{v(n)^2}{2v_0^2} \right)^{\frac{1}{2}} +$$

$$\frac{1}{2} d_0 \rho s A v(n)^3 + mgv(n) \sin \tau_c(n), \quad (10)$$

where v(n) is the 3D velocity at time slot n defined as:

$$v(n) = \frac{||\boldsymbol{\ell}(n+1) - \boldsymbol{\ell}(n)||}{\delta(n)},\tag{11}$$

 $\tau_c(n)$  denotes the climb angle, which is a function of  $\ell(n)$ , and the rest of parameters are defined in the aforementioned references. Finally, other constraints related to the UAV locations include a minimum and maximum flying altitude, the initial and final positions and a maximum velocity constraint:

$$H_{\min} \le H(n) \le H_{\max} \tag{12}$$

$$\ell(1) = \ell_i, \qquad \ell(N) = \ell_f, \tag{13}$$

$$||\boldsymbol{\ell}(n+1) - \boldsymbol{\ell}(n)|| \le V_{\text{max}}\delta(n). \tag{14}$$

# E. Sensing

The goal of sensing is to collect data from different events. Indeed, optimizing the UAV's trajectory will improve the efficiency and accuracy of the sensing. Particularly, we consider M events and utilize the probabilistic sensing model [33]–[35] where the dependency between sensing probability and UAV trajectory is through a distance-based exponential function. In other words, the probability of sensing event m at time n is

$$P_m(n) = e^{-\mu d_m(n)},$$
 (15)

where  $\mu$  determines the sensing capability of the UAV. Other relevant sensing models can be found in [13]. However, note that (15) avoids the dependency with respect to the time-slot length, i.e., longer  $\delta(n)$  might provide better sensing accuracy. In this work, we also study the impact of a time-dependent sensing probability. Inspired by [29], assume that the nth time slot is divided into X sub-slots of equal length  $t_n$ , i.e.,  $\delta(n) = Xt_n$ , and that the UAV carries out X trials to sense an event. A failure in the sensing occurs when all X trials fail to correctly sense the event. Hereby, the probability of successful sensing can be obtained through its complementary:

$$P_m(n) = 1 - \left(1 - e^{-\mu d_m(n)}\right)^{\frac{\delta(n)}{t_n}},$$
 (16)

where (i) a longer  $\delta(n)$  results in a higher probability and (ii)  $\delta(n) \geq t_n$  to ensure at least one trial. In addition, only one event can be sensed at a time, modeled by

$$0 \le \sum_{m=1}^{M} \alpha_m(n) \le 1. \tag{17}$$

Moreover, the sensing of the M events follows a certain order, discussed in Sec. IV-F, determined by  $S = \{s_1, \dots, s_M\}$  with  $s_m \in \mathcal{M}$ . Therefore, the following constraints must be met

$$\sum_{i=1}^{n} \left( \alpha_{s_m}(i) - \alpha_{s_j}(i) \right) \ge 0 \quad \text{for } m < j.$$
 (18)

Furthermore, it is required to sense each event once, which can be mathematically modeled by

$$\sum_{n=1}^{N} \alpha_m(n) = 1, \tag{19}$$

where a certain amount of data,  $C_m$ , is assumed to be generated by the UAV if  $\alpha_m(n) = 1$ . Altogether, based on the logic variables  $\alpha_m(n)$ , the constraint that must be met in terms of sensing probability is

$$P_{\text{s,th}} \le \alpha_m(n)P_m(n) + A(1 - \alpha_m(n)), \tag{20}$$

where  $P_{\rm s,th}$  is the minimum sensing probability the UAV requires to correctly sense an event and A is chosen to be a constant larger than  $P_{\rm s,th}$ . Note that a sensing variable can be active, i.e.,  $\alpha_m(n)=1$ , if  $P_m(n)\geq P_{\rm s,th}$ . To the contrary, if  $\alpha_m(n)=0$ , (20) is satisfied since  $A\geq P_{s,th}$ .

## F. Causality of the information

As stated in the introduction, compared to the existing works in the literature, the constraint that relates to the causality of the information needs to be redefined given that (i) the UAV uses the same resource block at all times without any time or frequency scheduling, and (ii) there is no link between the events and UAV. In fact, upon sensing an event, the UAV generates the sensory data, e.g. a picture or a measurement among others. Let us assume the UAV senses the events in a certain order, as defined by  $\mathcal S$  in Section II-E, and the amount of data generated by the  $s_m$ th event is  $C_{s_m}$ . Successful reception of the sensory data at the BS is ensured by the following sensing constraints:

$$\alpha_{s_{M}}(n) \sum_{i=n+D}^{N} \delta(i)R(i) + B(1 - \alpha_{s_{M}}(n)) \ge C_{s_{M}}$$

$$\vdots ,$$

$$\alpha_{s_{1}}(n) \sum_{i=n+D}^{N} \delta(i)R(i) + B(1 - \alpha_{s_{1}}(n)) \ge \sum_{m=1}^{M} C_{s_{m}}$$
(21)

where B is chosen to be a constant larger than  $\sum_{m=1}^{M} C_{s_m}$ . For example, before sensing any event or between two events, the binary variables are zero but the constraints are met due to  $B \geq \sum_{m=1}^{M} C_{s_m}$ . When the last event is sensed,  $\alpha_{s_M}(n) = 1$  and therefore after D samples, the amount of data that the BS

receives has to be larger than  $C_{s_M}$ . Whenever the penultimate event is sensed,  $\alpha_{s_{M-1}}(n)=1$  for  $n=n_{M-1}$ . Hence, the BS must be able to receive the data from the last two events in the last  $N-n_{M-1}-D$  samples. A similar procedure is followed to generate the causality constraints for the remaining events.

## III. PROBLEM FORMULATION

With the aim of producing energy-efficient trajectories for the sensing and communication problem, the objective function in our work is presented in Eq. (8). Constraints (4) and (7) determine the maximum transmit power and maximum GU interference, respectively. The set of constraints presented in (11)-(14) relate to the UAV mechanical capabilities and starting/ending point of the mission. In addition, introducing the set of logic variables  $\alpha_m(n)$  allows us to combine the communication and sensing constraints under the same umbrella. More specifically, constraints (17)-(21) ensure all M events are sensed and the corresponding sensory data is successfully received at the central BS. To this end, the optimization variables are: (i) sensing variables  $\alpha_m(n)$ , (ii) UAV trajectory (q(n), H(n)), (iii) length of the time slots  $\delta(n)$ , and (iv) transmit UAV power p(n). Therefore, the problem presented in (22) can be formulated, which falls within the class of nonconvex mixed-integer non-linear programming problems whose solution requires prohibitive time and computational complexity. Accordingly, we split the problem into four subproblems: (i) optimizing sensing with path, length of the time slots, and power fixed; (ii) optimizing 2D trajectory and time slot length with fixed sensing, altitude and power; (iii) optimizing altitude with sensing, 2D trajectory, length of the time slots, and power fixed; and (iii) optimizing power with sensing, path, and time slots fixed. Once the solution to each of the four subproblems is obtained, a BCD procedure [45] is followed until convergence is achieved.

## IV. JOINT OPTIMIZATION

In this section, we conduct a thorough analysis of the subproblems that arise from (22). More specifically, the optimization of the binary sensing variables is covered first. Second, an SCA-based approach for the joint trajectory and time slot optimization is presented. Finally, the optimal UAV transmit power can be derived through the Lagrangian method.

## A. Sensing Optimization

For fixed q(n),  $\delta(n)$ , H(n), and p(n), we first aim at solving the sensing optimization subproblem. Provided that the only contribution of the sensing variables,  $\alpha_m(n)$ , in the cost function is through the term that depends on the sensing power,  $p_s$ , the first optimization problem reduces to:

$$\min_{\alpha_m(n)} \quad \sum_{n=1}^{N} \sum_{m=1}^{M} \delta(n) \alpha_m(n) p_s$$
s.t. 
$$\alpha_m(n) \in \{0, 1\},$$

$$(17) - (21).$$
(23)

The binary nature of  $\alpha_m(n)$  results in an NP hard problem. Relaxing the binary assumption would result in constraint violations, and therefore the problem should be kept in the binary domain. To cope with the increased complexity, note that  $\alpha_m(n)=0$  when  $P_m(n)\leq P_{\rm s,th}$ . Hence, there is no need to search over the entire solution space, but only in the points satisfying  $P_m(n)\geq P_{s,th}$ . Consequently, the branch and cut is an appealing technique to solve this problem [52]. The complexity of this approach is discussed in Sec. IV-E

## B. Trajectory and Slot Length Optimization

Given any feasible  $\alpha_m(n)$ , H(n) and p(n), optimizing the 2D trajectory and the length of the time slots reduces to the following problem:

$$\min_{\mathbf{q}(n),\delta(n)} \quad \sum_{n=1}^{N} \delta(n) \bigg( p_f \big( n, \boldsymbol{\ell}(n), \delta(n) \big) + \\ \sum_{m=1}^{M} \alpha_m(n) p_s \, + \, p(n) \bigg)$$
 s.t. 
$$(1), (7), (11) - (14), (20), (21),$$

which is nonconvex. Therefore, we leverage the SCA technique to create an approximated version of (24). To full-fill this goal, we first obtain an equivalent problem by adding different slack variables such as  $\Delta(n) = ||\ell(n+1) - \ell(n)||$ . Given that  $v(n) = \frac{\Delta(n)}{\delta(n)}$ , the first term in the cost function can be re-written as:

$$\sum_{n=1}^{N} \delta(n) p_f(n, \ell(n), \delta(n)) = \sum_{n=1}^{N} P_0 \left( \delta(n) + \frac{3\Delta(n)^2}{U_{tip}^2 \delta(n)} \right) + P_i y(n) + \frac{1}{2} d_0 \rho s A \frac{\Delta(n)^3}{\delta(n)^2} + mg \Delta(n) \sin \tau_c(n),$$
(25)

where y(n), being a second slack variable, is defined below:

$$y(n)^{2} = \sqrt{\delta(n)^{4} + \frac{\Delta(n)^{4}}{4v_{0}^{4}}} - \frac{\Delta(n)^{2}}{2v_{0}^{2}}.$$
 (26)

After some algebraic manipulations over the previous equation, we have

$$\frac{\Delta(n)^4}{y(n)^2} = y(n)^2 + \frac{\Delta(n)^2}{v_0^2}.$$
 (27)

Finally, a third slack variable is needed to deal with the raterelated constraints:

$$\beta(n)^2 = \delta(n)R(n). \tag{28}$$

Consequently, the set of constraints in (21) can be expressed as a function of  $\beta(n)$  in a compact manner for a given event sensing order  $S = \{s_1, \ldots, s_M\}$ :

$$\alpha_{s_m}(n) \sum_{i=n+D}^{N} \beta(i)^2 + B(1 - \alpha_{s_m}(n)) \ge \sum_{l=m}^{M} C_{s_l}.$$
 (29)

As a result, the problem in (24) can be re-written as presented in (30).

**Proposition 1.** The optimization problems presented in (24) and (30) are equivalent.

$$\min_{\alpha_{m}(n), \mathbf{q}(n), H(n), \delta(n), p(n)} \quad \sum_{n=1}^{N} \delta(n) \left( p_{f}(n, \boldsymbol{\ell}(n), \delta(n)) + \sum_{m=1}^{M} \alpha_{m}(n) p_{s} + p(n) \right) \\
\text{s.t.} \quad \alpha_{m}(n) \in \{0, 1\}, \\
(1), (4), (7), (11) - (14), (17) - (21),$$
(22)

$$\min_{\mathbf{q}(n),\delta(n),\Delta(n),y(n),\beta(n)} \quad \sum_{n=1}^{N} P_0 \left( \delta(n) + \frac{3\Delta(m)^2}{U_{tip}^2 \delta(n)} \right) + P_i y(n) + \frac{1}{2} d_0 \rho_s A \frac{\Delta(n)^3}{\delta(n)^2} \\
+ mg \Delta(n) \sin \tau_c(n) + \sum_{n=1}^{N} \delta(n) \left( \sum_{m=1}^{M} \alpha_m(n) p_s + p(n) \right) \\
\text{s.t.} \quad \frac{\beta(n)^2}{\delta(n)} \leq R(n), \\
\frac{\delta(n)^4}{y(n)^2} \leq y(n)^2 + \frac{\Delta(n)^2}{v_0^2}, \\
||\ell(n+1) - \ell(n)|| \leq \Delta(n), \\
(1), (7), (11), (13), (14), (20), (29).$$
(30)

Proof. The proof can be found in App. A.

Still, some of the constraints in (30) are nonconvex which makes SCA relevant in this work. More precisely, SCA (a) locally convexifies the initial problem and (b) solves a convex approximated version by alternating between two steps: (i) upper (lower) bound a concave (convex) function by its first-order Taylor expansion and (ii) find the optimal solution of the approximated convex problem. In the subsequent, we derive the necessary approximations for the nonconvex constraints in (30). For ease of exposition, we denote variables by x and the value of the variable in the approximation point by  $\overline{x}$  and first cope with the expressions that relate to R(n).

**Proposition 2.** R(n) is jointly convex with respect to  $e^{-(B_1+B_2u_B(n))}$  and  $d_B^2(n)$ .

*Proof.* The proof can be found in App. B.

Using Prop. 2, the following lower bound for R(n) can be derived as a function of  $\lambda(n) = B_1 + B_2 u_B(n)$  and q(n).

**Lemma 1.** At any local point for the UAV trajectory  $\overline{q}(n)$  and  $\overline{\lambda}(n)$ , R(n) accepts the following lower bound:

$$R(n) \ge R^{lb}(n)$$

$$= \overline{R}(n) - \phi(n) \left( e^{-\lambda(n)} - e^{-\overline{\lambda}(n)} \right) -$$

$$\zeta(n) \left( ||\boldsymbol{q}(n) - \boldsymbol{q}_B||^2 - ||\overline{\boldsymbol{q}}(n) - \boldsymbol{q}_B||^2 \right).$$
 (32)

*Proof.* The proof and the values of  $\phi(n)$  and  $\zeta(n)$  can be found in App. C.

Hence, the constraint related to R(n) in (30) is locally convex given  $R^{lb}(n)$ . However, provided that  $\lambda(n)$  is nonconvex with respect to  $u_B(n)$ , since  $u_B(n) = \frac{(H(n) - H_B)}{d_B(n)}$ , a lower-bound for  $u_B(n)$  is required.

**Lemma 2.** At any local point for the UAV trajectory  $\overline{q}(n)$ ,  $u_B(n)$  accepts the following lower bound:

$$u_B(n) \ge u_B^{lb}(n)$$

$$= \overline{u}_B(n) - \psi(n) (||\boldsymbol{q}(n) - \boldsymbol{q}_B||^2 - ||\overline{\boldsymbol{q}}(n) - \boldsymbol{q}_B||^2).$$
(34)

*Proof.* The proof and the value of  $\psi(n)$  can be found in App. D.

Therefore, the constraint that  $\lambda(n)$  must satisfy is

$$\lambda(n) \le B_1 + B_2 u_B^{lb}(n). \tag{35}$$

The set of constraints that takes into account the maximum interference tolerated by out-of-central cell GUs is also non-convex with respect to q(n). However, an upper bound on the interference can be derived by considering the worst-case scenario of the UAV flying on top of User k:

$$\left(C_1 + \frac{C_2}{1 + e^{-(B_1 + B_2 u_k(n))}}\right) \frac{\beta_0 p(n)}{d_k^n(n)} \le I_k^{ub},$$
(36)

where

$$I_k^{ub} = \left(C_1 + \frac{C_2}{1 + e^{-B_1 - B_2}}\right) \frac{\beta_0 p(n)}{d_k^{\kappa}}.$$
 (37)

Following the previous equation and rearranging terms, we obtain

$$||q(n) - w_k||^2 \ge \left(\frac{(C_1 + \frac{C_2}{1 + e^{-B_1 - B_2}})\beta_0 p(n)}{I_{\text{th}}}\right)^{\frac{2}{\kappa}} - H^2,$$
(38)

which is still non-convex. Further application of the SCA results in:

$$||\overline{\boldsymbol{q}}(n) - \boldsymbol{w}_{k}||^{2} + 2(\overline{\boldsymbol{q}}(n) - \boldsymbol{w}_{k})^{T}(\boldsymbol{q}(n) - \overline{\boldsymbol{q}}(n)) \geq \left(\frac{(C_{1} + \frac{C_{2}}{1 + e^{-B_{1} - B_{2}}})\beta_{0}p(n)}{I_{\text{th}}}\right)^{\frac{2}{\kappa}} - H^{2}. \quad (39)$$

A similar procedure applies to (29), which results in the following convex set of constraints:

$$\alpha_{s_m}(n) \sum_{i=n+D}^{N} \left( \overline{\beta}(i)^2 + 2\overline{\beta}(i) \left( \beta(i) - \overline{\beta}(i) \right) \right) + B\left( 1 - \alpha_{s_M}(n) \right) \ge \sum_{l=m}^{M} C_{s_l}.$$
 (40)

Armed with the respective upper or lower bounds and after applying the same technique to the expressions that involve  $y(n)^2$ ,  $\Delta(n)^2$ , and, if needed (16), the local approximation of the problem in (30) is introduced in (41), where, compared to (30), we add  $c_z \le 1$  given that  $\sin \tau_c(n) \le 1$  and the sinfunction is neither convex nor concave. It can be verified that both the cost function and the constraints in (41) are convex. Therefore, (41) can be solved using standard optimization solvers such as CVX [53].

# C. Altitude Optimization

A similar methodology is followed to optimize the altitudes, H(n). Given the space limitations, we skip some derivations since the process is very similar to the 2D optimization. Consequently, the approximated optimization problem for the altitude is presented in (42), where  $R^{lb}(n)$ , (35), and (39) are slightly modified to account for the gradients w.r.t. to the altitude. Finally, (42) is a convex optimization problem and therefore can be efficiently solved [53].

## D. Power Allocation

The last subproblem aims at finding the optimal power allocation for given feasible  $\alpha_m(n)$ , q(n),  $\delta(n)$ , and H(n). The terms that include p(n) in the cost function and constraints result in

$$\min_{p(n)} \quad \sum_{n=1}^{N} \delta(n) p(n) 
\text{s.t.} \quad (4), (7), (21),$$

which is convex and can be analytically solved applying the Lagrangian method.

**Proposition 3.** The optimal power allocation for the UAV is given by

$$p^*(n) = \begin{cases} 0 & n = 1, \dots, D \\ \left[a(n) - \frac{1}{K_B(n)}\right]^+ & n = D + 1, \dots, N, \end{cases}$$
(44)

where a(n) depends on the Lagrangian multipliers and is defined in Eq. (62),  $K_B(n) = \left(C_1 + \frac{C_2}{1 + e^{-(B_1 + B_2 u_B(n))}}\right) \frac{\beta_0}{\sigma^2 d_B^{\kappa}(n)}$ , and the operator  $[x]^+ = \max(x, 0)$ .

*Proof.* The proof can be found in App. E.

# E. Algorithm Analysis

Based on the solutions to the previous subproblems, we propose an iterative method for the initial nonconvex problem in which we optimize four sets of variables: sensing variables, 3D UAV trajectories, time slot length, and power allocation. The convergence of the proposed BCD approach in Alg. 1 is guaranteed by the following proposition.

**Proposition 4.** The sequence of objective values generated by Alg. 1 is monotonically non-increasing with a lower bound, and therefore converges.

Proof. The proof can be found in App. F. 

# Algorithm 1 BCD updates for the optimization variables

Require: Initial sensing, trajectory, time slots and power variables at the first iteration, j = 0, given by  $\{\alpha_m^{(0)}(n), \boldsymbol{q}^{(0)}(n), \delta^{(0)}(n), H^{(0)}(n), p^{(0)}(n)\}$  and define by  $\eta^{(0)}$  the respective cost function.

while 
$$\frac{|\eta^{(j+1)} - \eta^{(j)}|}{\eta^{(j)}} > \epsilon$$
 do

Fix  $\{q^{(j)}(n), \delta^{(j)}(n), H^{(j)}(n), p^{(j)}(n)\}$  and solve (23) to obtain  $\{\alpha_m^{(j+1)}(n)\}$ .

Fix  $\{\alpha_m^{(j+1)}(n), H^{(j)}(n), p^{(j)}(n)\}$  and solve (30) to obtain  $\{q^{(j+1)}(n), \delta^{(j+1)}(n)\}$ .

Fix  $\{\alpha_m^{(j+1)}(n), q^{(j+1)}(n), \delta^{(j+1)}(n)\}$  and

solve (42) to obtain  $\{H^{(j+1)}(n)\}.$ 

Fix  $\{\alpha_m^{(j+1)}(n), \boldsymbol{q}^{(j+1)}(n), \delta^{(j+1)}(n), H^{(j+1)}(n)\}$  and solve (43) to obtain  $\{p^{(j+1)}(n)\}.$ 

Compute the cost function  $\eta^{(j+1)}$ .

## end while

The complexity of the previous algorithm is given by the combination of individual complexities for solving each of the subproblems. Particularly, it can be shown via induction that, given a sensing order, the maximum number of combinations for  $\alpha_m(n)$  in (23) is upper bounded by  $\sum_{i=1}^{N+M-1} (N-M+2)i$ , corresponding to the case in which the M events can be sensed during the N time slots, i.e., a very conservative bound. Additionally, given that (41) involves logarithmic forms, the interior point method presents a complexity of  $\mathcal{O}((7N)^{3.5}\log(1/\epsilon_1))$ where  $\epsilon_1$  relates to the convergence accuracy [54]. Similarly, solving (42) has a complexity of  $\mathcal{O}((5N)^{3.5}\log(1/\epsilon_2))$ . Finally, solving (43) has a complexity of  $\mathcal{O}((N+N^2)\log(1/\epsilon_3))$ where the term in  $N^2$  arises after applying the ellipsoid to the dual problem [53]. Consequently, the overall complexity is dominated by the SCA-based subproblems.

# F. Algorithm Initialization

Given initial and final trajectory points, the first step is to determine the sensing order S. Different criteria may apply, e.g. based on priority, distance or random. In our case, we set the ordering based on distance. Consequently,  $s_1 =$  $\arg\min_{m} ||\boldsymbol{\ell}(1) - \boldsymbol{\ell}_{m}|| \text{ while } s_{i+1} = \arg\min_{m} ||\boldsymbol{\ell}_{s_{i}} - \boldsymbol{\ell}_{m}||$ for  $m \neq s_i$ ,  $j \leq i$ . Next, the value of  $D_{\text{max}}$  is obtained, serving as an upper bound on the maximum distance the UAV has to cover, i.e.,  $D_{\max} \geq ||\boldsymbol\ell(1) - \boldsymbol\ell_{s_1}|| + \sum_{i=1}^{M-1} ||\boldsymbol\ell_{s_i} - \boldsymbol\ell_{s_i}||$  $\ell_{s_{i+1}}||+||\ell_{s_M}-\ell(N)||$ . As a consequence, for a fixed  $d_{\max}$ , the number of slots can be set as  $(N+1)d_{\max} >> D_{\max}$ . Next, we turn to generating the UAV trajectory. Initially, the UAV path coordinates will lie on the lines joining the departure point, events locations, and the destination point. Therefore,

$$\begin{split} \min_{\substack{q(n),\delta(n),\Delta(n),\\y(n),\beta(n),\tau(n)}} & \sum_{n=1}^{N} P_0 \Bigg( \delta(n) + \frac{3\Delta(m)^2}{U_{tip}^2 \delta(n)} \Bigg) + P_i y(n) + \frac{1}{2} d_0 \rho s A \frac{\Delta(n)^3}{\delta(n)^2} + mg \Delta(n) c_z \\ & + \sum_{n=1}^{N} \delta(n) \Bigg( \sum_{m=1}^{M} \alpha_m(n) p_s + \sum_{m=1}^{M} p(n) \Bigg) \\ \text{s.t.} & \frac{\beta(n)^2}{\delta(n)} \leq R^{lb}(n), \\ & \frac{\delta(n)^4}{y(n)^2} \leq \overline{y}(n)^2 + 2\overline{y}(n) \big( y(n) - \overline{y}(n) \big) + \\ & \frac{1}{v_0^2} \bigg( \overline{\Delta}(n)^2 + 2\overline{\Delta}(n) \big( \Delta(n) - \overline{\Delta}(n) \big) \bigg), \\ & (1), (11), (13), (14), (20), (35), (39), (40). \end{split}$$

$$\min_{\substack{H(n),\Delta(n),\\y(n),\beta(n),\tau(n)}} \quad \sum_{n=1}^{N} P_0 \left( \delta(n) + \frac{3\Delta(m)^2}{U_{tip}^2 \delta(n)} \right) + P_i y(n) + \frac{1}{2} d_0 \rho s A \frac{\Delta(n)^3}{\delta(n)^2} + mg \Delta(n) c_z$$
s.t.
$$\frac{\beta(n)^2}{\delta(n)} \leq R^{lb}(n),$$

$$\frac{\delta(n)^4}{y(n)^2} \leq \overline{y}(n)^2 + 2\overline{y}(n) (y(n) - \overline{y}(n)) +$$

$$\frac{1}{v_0^2} \left( \overline{\Delta}(n)^2 + 2\overline{\Delta}(n) (\Delta(n) - \overline{\Delta}(n)) \right),$$

$$(1), (12) - (14), (20), (35), (39), (40).$$

we ensure the initial trajectory is capable of sensing all events. Particularly, until the first event is sensed, i.e.,  $P_{s_1}(n) \geq P_{s, \text{th}}$  and therefore  $\alpha_{s_1}(n) = 1$ , the UAV coordinates lie on the line between the departure point and the first event as:

$$q_1(n+1) = q_1(n) + \alpha \sin \theta \cos \phi, \tag{45}$$

$$q_2(n+1) = q_2(n) + \alpha \sin \theta \sin \phi, \tag{46}$$

$$H(n+1) = H(n) + \alpha \cos \theta, \tag{47}$$

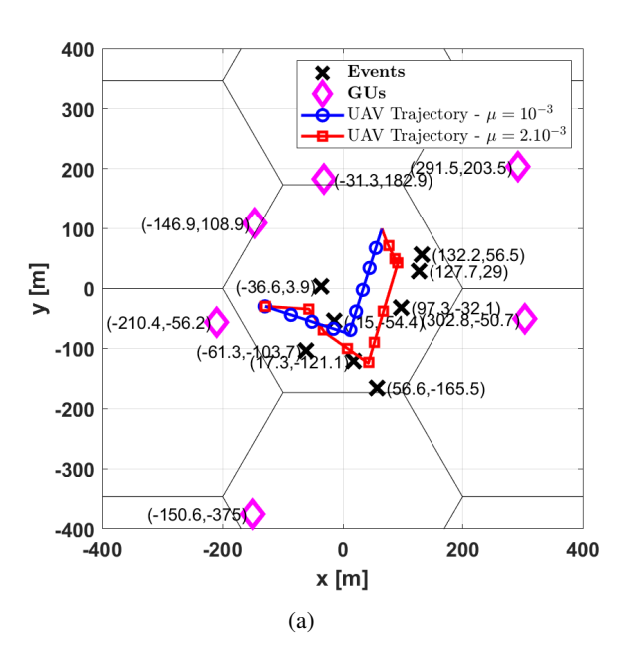
where  $\theta$  and  $\phi$  are the inclination and azimuth angles between  $\ell_i$  and  $\ell_{s_1}$ , respectively. The trajectory between two events lies on the line connecting the location where the former is sensed and the subsequent, with the corresponding recalculation of  $\theta$  and  $\phi$  while satisfying the altitude constraints. Finally, after sensing  $s_M$ , the same formulation applies with the angles corresponding to the points associated to  $\ell_{s_M}$  and  $\ell_f$ . To maintain the accuracy in the sampling while satisfying the maximum velocity constraint, we have  $\alpha \leq \min\{d_{\max}, V_{\max}\delta(n)\}$ . Once the trajectory and sensing variables are initialized, the powers are set to the minimum value between  $p_{\max}$  and the value that satisfies the interference constraint (7). To verify that the causality constraints are met, a search is performed. Otherwise, either more slots can be added or the problem can be declared infeasible.

# V. NUMERICAL RESULTS

For the purpose of performance evaluation, we consider a cellular network composed by one central and six neighboring cells, each following a hexagonal shape of radius R=200m,

although our work is independent of the cell shape. Unless otherwise specified, Table I lists the parameters used in the simulations, selected from the UAV and sensing literature [12], [15], [26]. Observe that the parameters related to Eq. (8) are not included since they are the same as the ones in [21]. To maintain the accuracy in the path discretization process, we consider  $d_{\text{max}} = 2$  and an upper bound on the flying distance  $D_{\text{max}} = 400\text{m}$ . Therefore,  $(N+1)d_{\text{max}} > D_{\text{max}}$  is satisfied with N > 300. In this case, we use N = 400 where the initial length of the slots is  $\delta(n) = 0.25$ s with a resulting initial flying time of T = 100s. The typical scenario that we use in our simulations and the corresponding events and GU locations are presented in Fig. 2a, with M=8 events and K=6 GUs, i.e., one per each neighboring cell. The starting and final points are  $\ell_i = [130, -30, 50]$  and  $\ell_f = [65, 100, 50]$ , respectively. The UAV trajectory for two cases of  $\mu = 10^{-3}$ and  $\mu = 2 \cdot 10^{-3}$  using the above typical scenario is included in Figs. 2a and 2b, with the former showing the 2D projection and the latter plotting the 3D trajectories to gain intuition on the altitude variations. Though more insight will be provided about the influence of  $\mu$ , it is shown that higher values, i.e., worse sensing capability, require the UAV to fly closer to the events. In fact, from Fig. 2b it can be shown that the UAV tends to fly at lower altitudes for  $\mu = 2 \cdot 10^{-3}$  to satisfy the sensing requirements compared to  $\mu = 10^{-3}$ .

We first verify Prop. 4 in Fig. 3 for different initializations and BCD orderings. Particularly, in O1, the optimization order in Alg. 1 is:  $\{\alpha_m(n), q(n), \delta(n), H(n), p(n)\}$  whereas in O2,



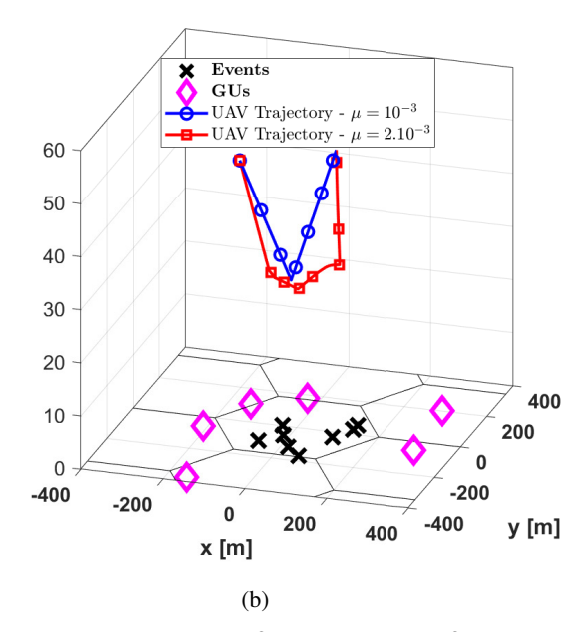


Fig. 2: Typical scenario with M=8 events, K=6 GUs, and the UAV trajectory for  $\mu=10^{-3}$  and  $\mu=2\cdot 10^{-3}$ ; (a) 2D, (b) 3D.

TABLE I: Simulation Parameters

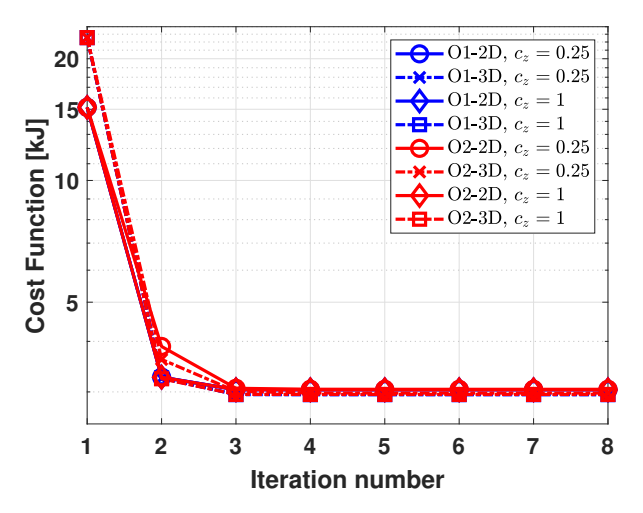
Description	Parameter	Value
Path loss at 1 m	$\beta_0$	-30 dB
Path loss exponent	$\kappa$	2
Logistic regression parameters	$C_1, C_2$	0, 1
Logistic regression parameters	$B_1, B_2$	-4.3221, 6.0750
BS altitude	$H_{ m B}$	25 m
Noise power	$\sigma^2$	-96 dBm
Minimum sensing probability	$P_{ m s,th}$	0.9
Maximum UAV transmit power	$p_{\mathrm{max}}$	100 mW
Maximum GU interference	$I_{ m th}$	-73 dBm
Maximum UAV velocity	$V_{ m max}$	30 m/s
Sensing capability at the UAV	$\mu$	$10^{-3}$
Processing delay	D	1
Sensing power	$p_s$	0.1 mW

the optimization order is  $\{H(n), \mathbf{q}(n), \delta(n), p(n), \alpha_m(n)\}.$ In addition, 2D initializes the altitude at a constant value H(n) = 50m while 3D uses the method described in Sec. IV-F. Finally, different values of  $c_z$  are tested as well to see its effect in the final solution. First, note that no matter what ordering and initialization setup we utilize, convergence in Alg. 1 is achieved only after a few iterations. Additionally, the difference in terms of cost function is minimal. However, the solutions differ. This can be seen in Fig. 4, where for a variety of initializations, the UAV altitudes may be different though requiring a similar energy budget. Such a tendency is mainly because all methods converge to a solution where the UAV flies at the velocity that minimizes the required energy, as described in [21, Sec. II-B]. More details on this phenomena are provided in subsequent paragraphs where the UAV velocity is also a matter of study.

Next, in Figs. 5a and 5b we compare the energy and flying time, respectively, for different benchmarks parametrized by M. Particularly, "Proposed" stands for the algorithm presented in this work while "Min-Time" solves the flying time

minimization problem. Additionally, "Equal- $\delta(n)$ " utilizes a similar algorithm as ours, but with fixed  $\delta(n) = 0.25s$  for all n. Finally, the "Max-Vel" benchmark is an heuristic algorithm based on the one described in Sec. IV-F, where the UAV flies at maximum velocity between each pair of points ensuring the rest of constraints are met. As expected, the more events, i.e., increasing M, the higher the energy and flying times are. Clearly, in terms of required on-board energy, our method outperforms the rest of benchmarks by saving at least 25% of the energy, whereas the minimum flying time is attained by the "min-Time" benchmark, with our method being close. Note that given the correlation between the "Proposed" and "min-Time" algorithms, their performance is similar, where shorter flying time results in less energy. In addition, the gap between the "Proposed" and "Equal- $\delta(n)$ " curves arises by adding  $\delta(n)$  into the optimization problem. Therefore, it is clear that non-uniform slots make a big difference in terms of energy-efficiency and flying time given the added degrees of freedom and the enlarged feasibility region compared to a fixed time slot.

Fig. 6 studies the impact of N in the simulation environment for the proposed algorithm and a variety of benchmarks. While Figs. 6a and 6b plot the energy and flying time, respectively, parametrized by N, Fig. 6c presents the UAV velocity for N=400 under three algorithms. It can be concluded from Figs. 6a and 6b that the methods that include  $\delta(n)$  in the optimization, i.e., "Proposed" and "Min-Time", converge to the same cost function independent of the value of N. This is in conjunction with the flying velocities presented in Fig. 6c, where the "Proposed" method adjusts the UAV path to fly at the velocity that minimizes the energy, as explained in [21, Sec. II-B], achieved if v(n)=17.7 m/s. In addition, to minimize the flying time, the UAV flies at its maximum



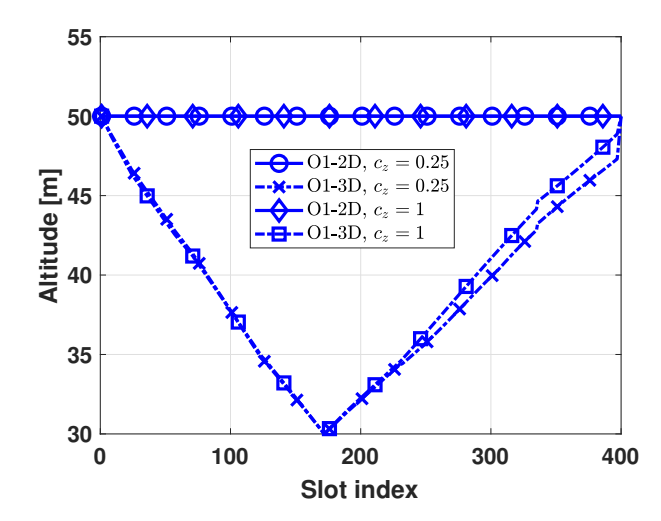
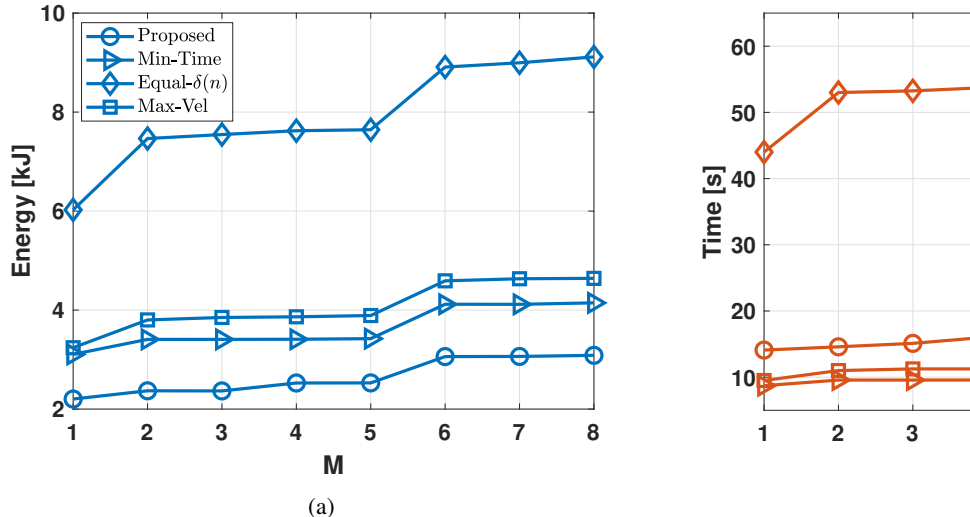


Fig. 3: Convergence of Prop. 4 for a variety of initializations, BCD orderings and  $c_z$ .

Fig. 4: Final UAV flying altitude for a variety of initializations and  $c_z$ .



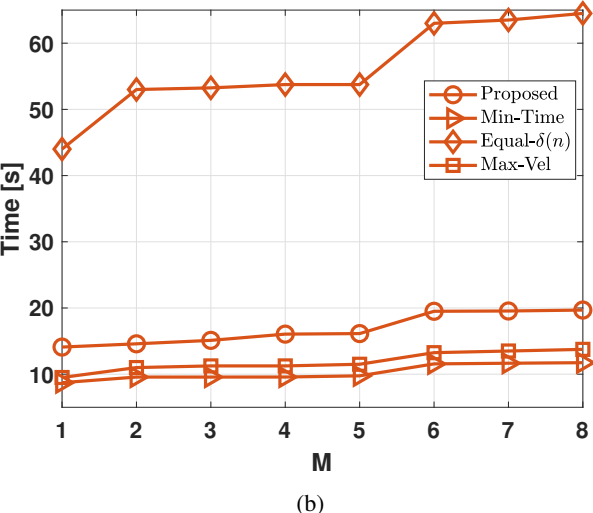


Fig. 5: (a) Energy and (b) flying time for different M and a variety of algorithms.

velocity, in this case v(n)=30 m/s. To the contrary, if  $\delta(n)$  is not included in the optimization: (i) the energy and flying time tend to be higher than the other methods and (ii) after a certain value of N, both energy and time stabilize given that adding more slots is no longer helpful. In this case, it can be concluded from the three pictures that N>260 does not provide any change given that the UAV can finalize its mission in less slots and therefore will hover at the destination point spending unnecessary energy.

Fig. 7 examines the dependency of the amount of needed energy and time to complete the sensing mission with respect to the sensing probability,  $P_{\rm s,th}$ . The blue curves correspond to the required energy while the red curves relate to the flying time. Figs. 7a and 7b utilize the model in (15), with Fig. 7b considering a fixed flying altitude of H(n)=50m. Finally, Fig. 7c considers the model in (16). In addition, different values for the sensing capability,  $\mu$ , are also presented. Clearly, a smaller  $\mu$  allows the UAV to sense the events at larger

distances compared to a higher  $\mu$ , as shown in Figs. 2a and 2b. Therefore, the use of smaller  $\mu$  results in trajectories whose energy and time serve as a lower bound for higher values of  $\mu$ . Additionally, increasing the value of  $P_{s,th}$  requires the UAV to fly closer to the events. As a consequence, both energy and flying time tend to increase with the threshold probability. By comparing Figs. 7a and 7b, it is shown that for higher values of  $P_{\rm s.th}$ , optimizing the altitude, as in Fig. 7a, reduces the required energy and time given that the distance between the UAV and the event can be smaller if the UAV has freedom to adapt its altitude. Finally, the difference between the values in Figs. 7a and 7c is minimal. Although the latter considers a sensing model that depends on the length of the time-slot, i.e., higher  $\delta(n)$  results in a higher sensing probability, the energy and flying time mainly depend on the velocity. In fact, as shown in Fig. 7d, which plots the velocity for the models in (15) (solid-blue) and (16) (dashed-red), in both cases the UAV velocity converges to the value that minimizes the required

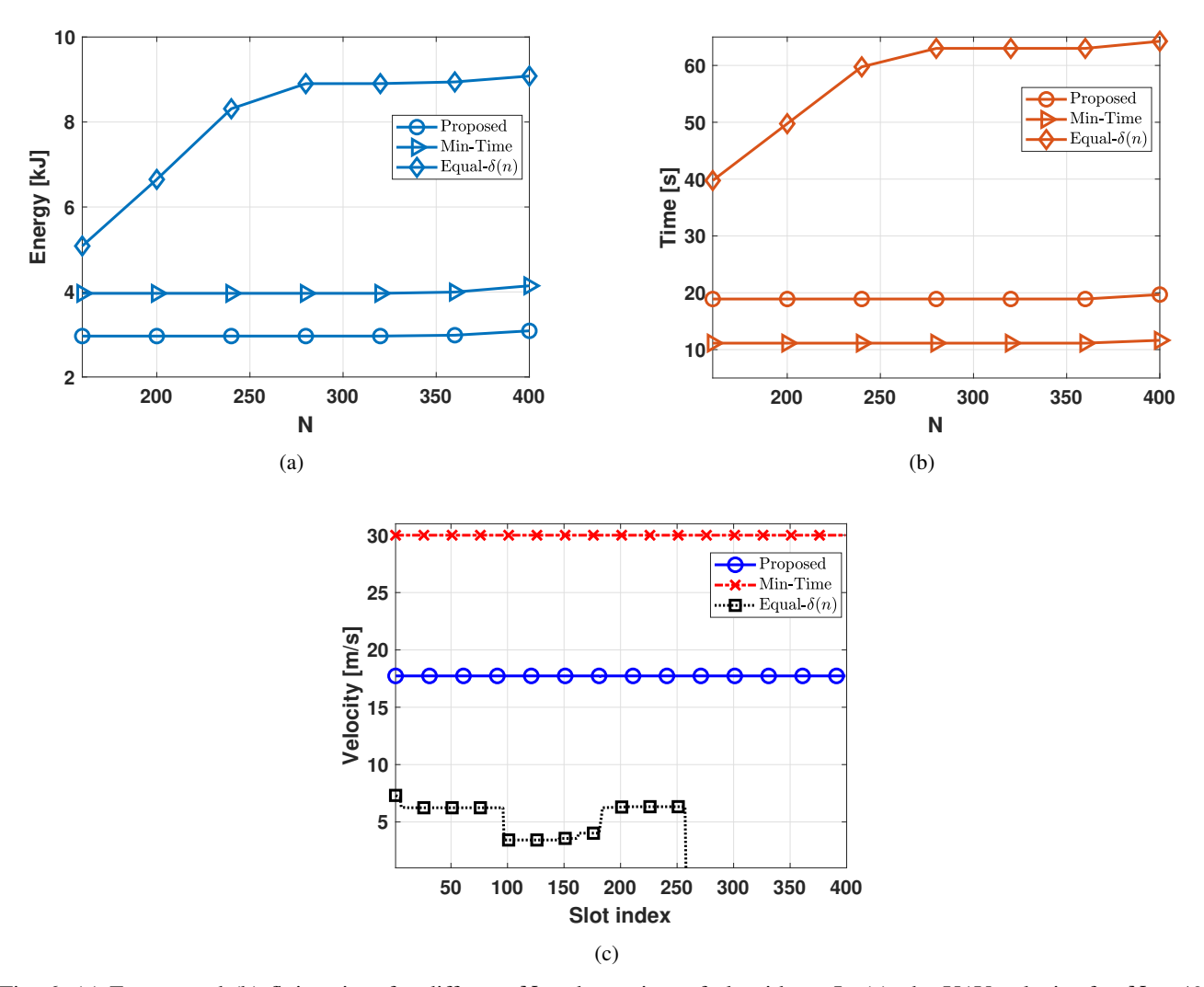


Fig. 6: (a) Energy and (b) flying time for different N and a variety of algorithms. In (c), the UAV velocity for N = 400.

energy, i.e., v(n) = 17.7 m/s. As a consequence, the energy and time obtained using (15) and (16) are similar.

Next, we study the effects of the maximum interference tolerated by the GUs, given by  $I_{\rm th}$ . In Figs. 8a and 8b, we present the variation of energy and time parametrized by  $I_{\mathrm{th}}$ , respectively. We present a variety of algorithms, as in previous figures. While the "Proposed" and "min-Time" refer to the same systems as in other figures, the "max-Vel" also adjusts the power as in (43) provided that the initialization algorithm might use more power than what is needed for the communication part. As in previous figures, the proposed method outperforms the rest in terms of required energy by at least 25% though needs more time to complete the mission. Additionally, given that the cost function is dominated by the flying energy, variations in the transmit power are not distinguishable in Fig. 8a. Second, in general, the amount of needed energy and time tend to increase as  $I_{\rm th}$  decreases given that the feasible regions shrink for decreasing  $I_{\rm th}$ . Note that for  $I_{\rm th} \to 0$ , the problem might be infeasible.

To gain more insight on the effects of interference, we include Fig. 9. Particularly, Fig. 9a plots the gap in the

interference constraint, defined as:

$$\Delta = \sqrt{||q(n) - w_k||^2 + H^2} - \sqrt{\left(\frac{(C_1 + \frac{C_2}{1 + e^{-B_1 - B_2}})\beta_0 p(n)}{I_{\text{th}}}\right)^{\frac{2}{\kappa}}}$$
(48)

for the GU at [302.8, -50.7]. The definition of  $\Delta$  arises from calculating the difference between the square root of the left and right hand sides of the constraint presented in (38). Note that in fact, (48) provides a notion on how (38) is met. Higher values of  $\Delta$  mean the UAV easily meets the constraint while smaller values of  $\Delta$  mean the UAV finds it harder to meet the interference constraint. More particularly, by looking at Fig. 9a, it can be verified that smaller  $I_{\rm th}$  yields a smaller  $\Delta$  since the regions where the UAV can fly, meeting the interference constraints, become smaller. In addition, note that in fact, the "min-Time" algorithm provides smaller  $\Delta$  given that higher transmit powers can still meet the constraints since its goal is to minimize the flying time, not the flying energy/power. Additionally, Figs. 9b and 9c plot the transmit power, p(n), for different values of  $I_{\rm th}$  using the "Proposed" and "min-Time" algorithms, respectively. Note that these curves compare

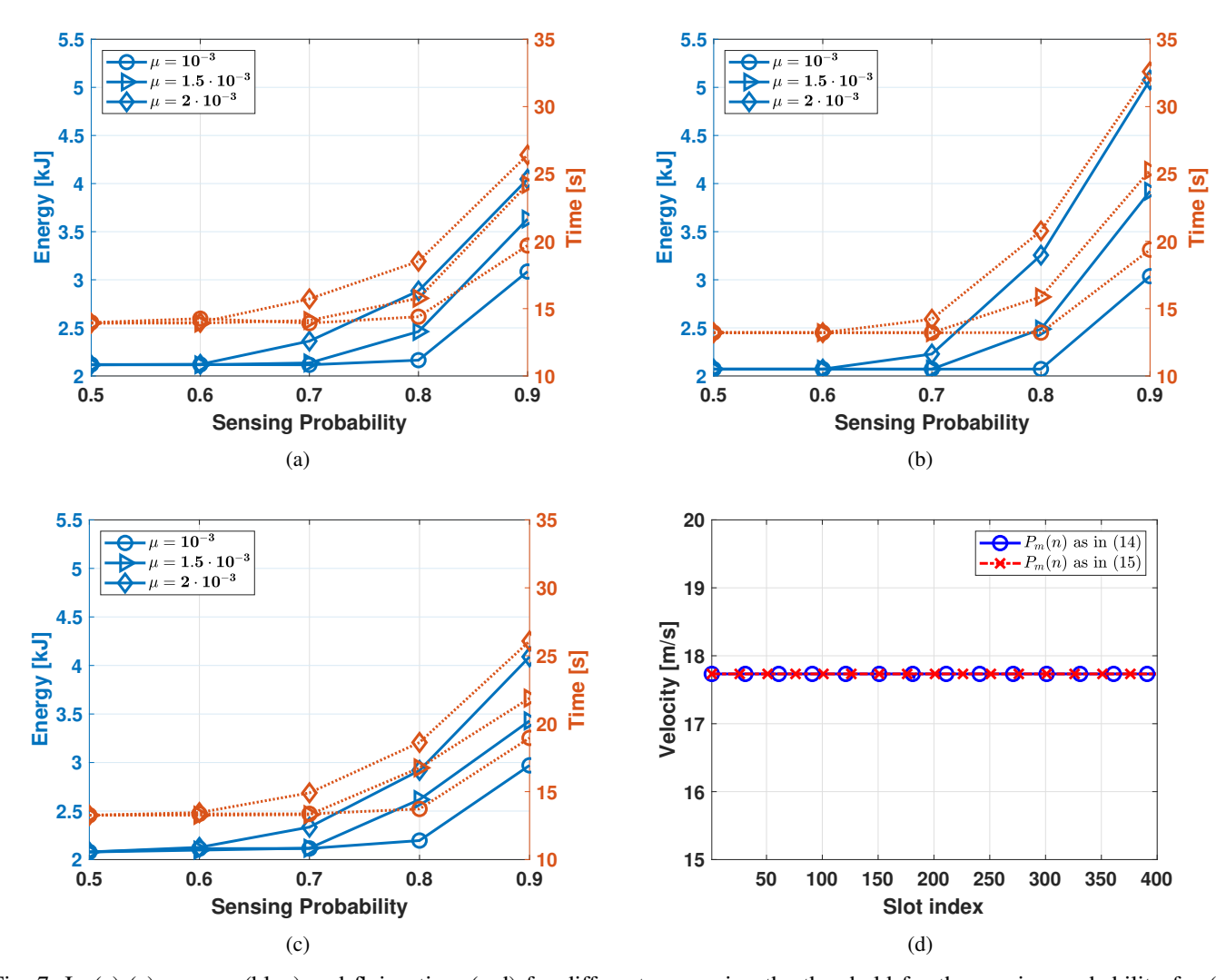


Fig. 7: In (a)-(c), energy (blue) and flying time (red) for different  $\mu$ , varying the threshold for the sensing probability for (a) sensing model in (15) with 3D optimization; (b) sensing model in (15) with 2D optimization; (c) sensing model in (16) with 3D optimization. In (d) velocity for  $\mu = 10^{-3}$  and  $P_{\rm s,th} = 0.9$ .

an easy-to-meet interference constraint, i.e.,  $I_{\rm th}=10^{-8}$ , versus limiting values of  $I_{\rm th}$ . More importantly, the orders of magnitude for the transmit power are very different in Figs. 9b and 9c. While the former adjusts its power to satisfy the communication requirements with minimum power, the latter does not perform power minimization, which yields to a much higher power consumption for communication purposes. Finally, the water-filling nature of the solution obtained in (43) can be verified from Fig. 9b. Between the slots 200 and 300, the UAV flies close to the BS. Therefore, it experiences favorable channel conditions which result in the increase of the transmit power.

## VI. CONCLUSIONS

This paper has considered energy-efficient communications and sensing where an aerial vehicle senses multiple events of interest. After generating the sensory data, the UAV ensures its reception by the BS while managing the interference effect to GUs located at neighboring cells. We have considered a generic cellular network with Rician channel models

and presented mechanical-related, communication-related, and sensing-related constraints that must be satisfied to complete the mission. We presented a novel logic-based approach to formulate (a) the 3D path planning, (b) sensing, and (c) transmit power subproblems. This formulation has allowed us to use classic optimization techniques. Most remarkably, we have studied the dependency of the UAV trajectory with respect to different parameters and benchmarks, namely: (i) maximum velocity, (ii) minimum flying time, and (iii) fixedslot duration. Comparative studies across various number of events have demonstrated that our proposed approach results in a reduction of energy consumption between 33%-50%. Moreover, the proposed scheme outperformed the minimum flying time and maximum velocity benchmarks by consuming 33%-41% less energy, depending on the maximum level of interference the GUs can tolerate. Finally, the number of time slots and time slot duration have a significant impact on overall performance. Our solution consumes 33% and 200% less energy compared to the minimum flying time and fixed-

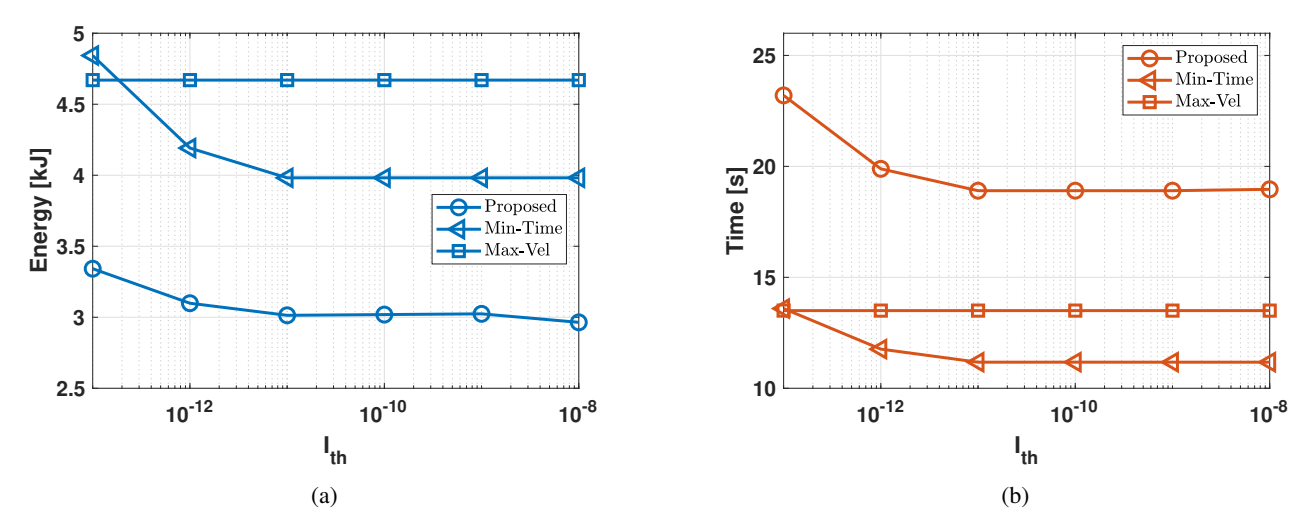


Fig. 8: Energy (solid/blue) and flying time (dot/red) for different  $I_{th}$  and for (a) H = 50m and (b) H = 30m.

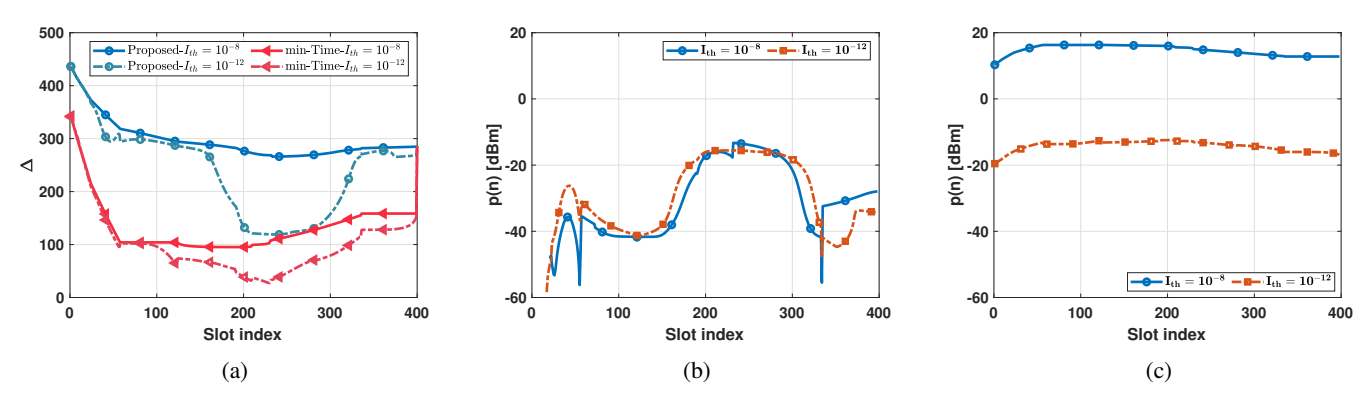


Fig. 9: For different values of  $I_{\rm th}$  and algorithms, (a)  $\Delta$ ; (b) p(n) for the "Proposed" algorithm; and (c) p(n) for the "Min-Time" algorithm.

slot duration benchmarks, respectively.

## APPENDIX A

Given that we have added three slack variables, we analyze their behavior individually. First,  $||\boldsymbol\ell(n+1)-\boldsymbol\ell(n)|| \leq \Delta(n)$  will be met with equality at the optimal, otherwise the value of  $\Delta(n)$  can be reduced to achieve a better cost function. A similar argument is used to show that  $y(n)^2 = \sqrt{\delta(n)^4 + \frac{\Delta(n)^4}{4v_0^4}} - \frac{\Delta(n)^2}{2v_0^2}$ , otherwise the value of y(n) can be decreased to reduce the cost function. Finally, at the optimal, Eq. (28) is met, or else the value of  $\beta(n)$  can be increased.

# APPENDIX B

We first define  $x=1+e^{-(B_1+B_2u_B(n))}$  and  $y=d_B^2(n)$ . Also, let us define  $C_3=C_1\frac{\beta_0p(n)}{\sigma^2}$  and  $C_4=C_2\frac{\beta_0p(n)}{\sigma^2}$ , both strictly positive for p(n)>0. Substituting the previous terms into R(n) and dropping the time index n, we obtain  $R=f(x,y)\log_2(e)$  where  $f(x,y)=\log\left(1+\left(C_3+\frac{C_4}{x}\right)\frac{1}{y^{\frac{n}{2}}}\right)$ . The Hessian matrix of f(x,y) is included in Eq. (49). For any vector  $\boldsymbol{s}=(s_1,s_2)^{\mathrm{T}}$ , it can be shown that  $\boldsymbol{s}^{\mathrm{T}}\nabla^2 f(x,y)\boldsymbol{s}\geq 0$  as included in Eq. (50). Therefore, f(x,y) is convex with

respect to x, y, which ultimately implies the convexity of R(n) as well.

# APPENDIX C

By exploiting the convexity of R(n) as shown in Prop. 2, such a term accepts a lower bound of the type:

$$R(n) \ge R^{lb}(n)$$

$$= \overline{R}(n) - \phi(n) \left( e^{-\lambda(n)} - e^{-\overline{\lambda}(n)} \right) -$$

$$\zeta(n) \left( ||\boldsymbol{q}(n) - \boldsymbol{q}_B||^2 - ||\overline{\boldsymbol{q}}(n) - \boldsymbol{q}_B||^2 \right),$$
 (51)

where coefficients  $\phi(n)$  and  $\zeta(n)$  are provided in Eqs. (52) and (53), respectively.

## APPENDIX D

A similar procedure as the one followed in App. B is considered to show the convexity of  $u_B(n) = \frac{(H(n) - H_B)}{d_B(n)}$  with respect to  $||\boldsymbol{q}(n) - \boldsymbol{q}_B||^2$ . As a consequence,  $u_B(n)$  accepts the following lower bound:

$$u_B(n) \ge u_B^{lb}(n)$$

$$= \overline{u}_B(n) - \psi(n) (||\boldsymbol{q}(n) - \boldsymbol{q}_B||^2 - ||\overline{\boldsymbol{q}}(n) - \boldsymbol{q}_B||^2),$$
(55)

$$\nabla^{2} f(x,y) = \begin{pmatrix} \frac{\partial^{2} f(x,y)}{\partial x^{2}} & \frac{\partial^{2} f(x,y)}{\partial x \partial y} \\ \frac{\partial^{2} f(x,y)}{\partial x \partial y} & \frac{\partial^{2} f(x,y)}{\partial y^{2}} \end{pmatrix} = \begin{pmatrix} \frac{C_{4}(2xy^{\frac{\kappa}{2}} + 2C_{3}x + C_{4})}{x^{2}(xy^{\frac{\kappa}{2}} + C_{3}x + C_{4})^{2}} & \frac{\frac{\kappa}{2}C_{4}y^{\frac{\kappa}{2} - 1}}{xy^{\frac{\kappa}{2}} + C_{3}x + C_{4})^{2}} \\ \frac{\frac{\kappa}{2}C_{4}y^{\frac{\kappa}{2} - 1}}{xy^{\frac{\kappa}{2}} + C_{3}x + C_{4})^{2}} & \frac{\frac{\kappa}{2}(C_{3}x + C_{4})\left((1 + \frac{\kappa}{2})xy^{\frac{\kappa}{2}} + C_{3}x + C_{4}\right)}{y^{2}(xy^{\frac{\kappa}{2}} + C_{3}x + C_{4})^{2}} \end{pmatrix}.$$
(49)

$$\begin{split} s^{\mathrm{T}} \nabla^2 f(x,y) s &= s_1^2 \frac{C_4 (2xy^{\frac{\kappa}{2}} + 2C_3 x + C_4)}{x^2 (xy^{\frac{\kappa}{2}} + C_3 x + C_4)^2} + s_2^2 \frac{\frac{\kappa}{2} (C_3 x + C_4) \left( (1 + \frac{\kappa}{2}) xy^{\frac{\kappa}{2}} + C_3 x + C_4 \right)}{y^2 (xy^{\frac{\kappa}{2}} + C_3 x + C_4)^2} + \frac{2s_1 s_2 \frac{\kappa}{2} C_4 y^{\frac{\kappa}{2} - 1}}{xy^{\frac{\kappa}{2}} + C_3 x + C_4)^2} = \\ &\qquad \qquad \frac{C_4 s_1^2 y^2 (xy^{\frac{\kappa}{2}} + 2C_3 x + C_4) + s_2^2 x^2 \left( (2C_3 x + C_4) xy^{\frac{\kappa}{2}} + (C_3 x + C_4)^2 \right) + C_4 xy^{\frac{\kappa}{2}} (s_1 y + s_2 x)^2}{x^2 y^2 (xy^{\frac{\kappa}{2}} + C_3 x + C_4)^2}. \end{split}$$

$$\phi(n) = \frac{\partial R(n)}{\partial (1 + e^{-\lambda(n)})} = \frac{\frac{\beta_0}{\sigma^2} p(n) C_2}{\log(2) (1 + e^{-\overline{\lambda}(n)}) \left(\frac{\beta_0}{\sigma^2} p(n) [C_1 (1 + e^{-\overline{\lambda}(n)}) + C_2] + (1 + e^{-\overline{\lambda}(n)}) d_B^{\kappa}(n)\right)}$$
(52)

$$\zeta(n) = \frac{\partial R(n)}{\partial d_B^2(n)} = \frac{\frac{\beta_0}{\sigma^2} p(n) \kappa [C_1(1 + e^{-\overline{\lambda}(n)}) + C_2]}{2 \log(2) d_B^2(n) (\frac{\beta_0}{\sigma^2} p(n) [C_1(1 + e^{-\overline{\lambda}(n)}) + C_2] + (1 + e^{-\overline{\lambda}(n)}) d_B^{\kappa}(n))}$$
(53)

where the value of  $\psi(n)$  is

$$\psi(n) = \frac{\partial u_B(n)}{\partial ||\mathbf{q}(n) - \mathbf{q}_B||^2}$$
 (56)

$$= \frac{H(n) - H_B}{2(||\overline{q}(n) - q_B||^2 + (H(n) - H_B)^2)^{\frac{3}{2}}}$$
 (57)

#### APPENDIX E

To solve the power allocation problem, we first formulate the Lagrangian as in (58). Defining  $w_m(n) = \sum_{i=1}^{n-D} \lambda_{i,m} \alpha_{s_m}(i)$ , the Lagrangian can be rewritten as presented in (59) where  $K_{ct}$  is a constant term that does not depend on p(n). Taking the derivative with respect to the optimization variables, p(n), for fixed values of the multipliers, we obtain

$$\frac{d\mathcal{L}(p(n), \lambda)}{dp(n)} = \delta(n) + \sum_{m=1}^{M} \frac{w_m(n)\delta(n)}{\ln(2)} \frac{K_B(n)}{1 + p(n)K_B(n)} - \sum_{k=1}^{K} \lambda'_{n,k} K_k(n) - \lambda''_{n,m} = 0.$$
(60)

Solving the previous equation for p(n), we obtain:

$$p(n) = \left[\frac{\sum_{m=1}^{M} \frac{w_m(n)\delta(n)}{\ln(2)}}{\sum_{k=1}^{K} \lambda'_{n,k} K_k(n) + \lambda''_n - \delta(n)} - \frac{1}{K_B(n)}\right]^+, \quad (61)$$

for all n = D + 1, ..., N. The value of a(n) in Eq. (44) is therefore:

$$a(n) = \frac{\sum_{m=1}^{M} \frac{w_m(n)\delta(n)}{\ln(2)}}{\sum_{k=1}^{K} \lambda'_{n,k} K_k(n) + \lambda''_n - \delta(n)}.$$
 (62)

To obtain the Lagrangian multipliers, we aim to solve the dual problem after obtaining the solution to p(n):

$$\max_{\lambda} \quad \mathcal{L}(p(n), \lambda)$$
s.t.  $\lambda \ge 0$ , (63)

which can be efficiently solved by gradient methods and therefore obtain the optimal multipliers  $\lambda^*$  for fixed  $p^*(n)$ . Particularly, the ellipsoid method is an enticing solution [53] where obtaining the subgradient of  $\mathcal{L}(p^*(n), \lambda)$  with respect to  $\lambda$  for fixed  $p^*(n)$  is a straightforward calculation given (59). Consequently, we use an iterative process between the solutions obtained in (61) and (63).

## APPENDIX F

Define the iteration number and the corresponding cost function by j and  $\eta^{(j)}$ , respectively. Note that  $\eta^{(j)}$  is a function of the optimization variables, i.e.,  $\eta(\alpha_m^{(j)}, \boldsymbol{q}^{(j)}, \delta^{(j)}, H^{(j)}, p^{(j)})$ , where, for ease of exposition, we get rid of the time index n. The BCD approach followed in Alg. 1 provides the following inequalities: (i)  $\eta(\alpha_m^{(j)}, \boldsymbol{q}^{(j)}, \delta^{(j)}, H^{(j)}, p^{(j)}) \geq \eta(\alpha_m^{(j+1)}, \boldsymbol{q}^{(j)}, \delta^{(j)}, H^{(j)}, p^{(j)})$  by solving (23); (ii) applying the SCA technique to the 2D-UAV path and UAV altitude subproblems presented in (30) and (42), respectively, results in  $\eta(\alpha_m^{(j+1)}, \boldsymbol{q}^{(j)}, \delta^{(j)}, H^{(j)}, p^{(j)}) \geq \eta(\alpha_m^{(j+1)}, \boldsymbol{q}^{(j+1)}, \delta^{(j+1)}, H^{(j+1)}, p^{(j)})$ , and (iii) optimizing the transmit power in (43) results in  $\eta(\alpha_m^{(j+1)}, \boldsymbol{q}^{(j+1)}, \delta^{(j+1)}, \delta^{(j+1)}, H^{(j+1)}, p^{(j)}) \geq \eta(\alpha_m^{(j+1)}, \boldsymbol{q}^{(j+1)}, \delta^{(j+1)}, \delta^{(j+1)}, H^{(j+1)}, p^{(j+1)})$ . As a result, Alg. 1 provides a non-increasing sequence:  $\eta^{(0)} \geq \eta^{(1)} \geq \cdots \geq \eta^{(*)}$  where for simplicity  $\eta^{(*)}$  is the objective function after convergence. Since the cost function is lower-bounded by a value of zero, the BCD approach followed by Alg. 1 will converge.

$$\mathcal{L}(p(n), \lambda) = \sum_{n=1}^{N} \delta(n) p(n) + \sum_{n=1}^{N-D} \sum_{m=1}^{M} \lambda_{n,m} \Big[ \alpha_{s_m}(n) \sum_{i=n+D}^{N} \delta(i) R(i) + B \Big( 1 - \alpha_m(n) \Big) - \sum_{l=m}^{M} C_{s_l} \Big] + \sum_{n=D+1}^{N} \sum_{k=1}^{K} \lambda'_{n,k} \Big( I_{th} - p(n) K_k(n) \Big) + \sum_{n=D+1}^{N} \lambda''_{n} \Big( p_{max} - p(n) \Big).$$
(58)

$$\mathcal{L}(p(n), \lambda) = \sum_{n=1}^{N} \delta(n)p(n) + \sum_{n=D+1}^{N} \sum_{m=1}^{M} w_m(n)\delta(n)R(n) - \sum_{n=D+1}^{N} \sum_{k=1}^{K} \lambda'_{n,k} p(n)K_k(n) - \sum_{n=D+1}^{N} \lambda''_n p(n) + K_{ct},$$
(59)

## REFERENCES

- F. Liu et al., "Integrated Sensing and Communications: Toward Dual-Functional Wireless Networks for 6G and Beyond," *IEEE Journal on Sel. Areas in Commun*, vol. 40, pp. 1728–1767, Mar. 2022.
- [2] T. Wild, V. Braun, and H. Viswanathan, "Joint Design of Communication and Sensing for Beyond 5G and 6G Systems," *IEEE Access*, vol. 9, pp. 30845–30857, Feb. 2021.
- [3] C. De Lima et al., "Convergent Communication, Sensing and Localization in 6G Systems: An Overview of Technologies, Opportunities and Challenges," *IEEE Access*, vol. 9, pp. 26902–26925, Jan. 2021.
- [4] J. Guo, P. Walk, and H. Jafarkhani, "Optimal Deployments of UAVs With Directional Antennas for a Power-Efficient Coverage," *IEEE Trans. Commun.*, vol. 68, pp. 5159–5174, Aug. 2020.
- [5] E. Koyuncu, M. Shabanighazikelayeh, and H. Seferoglu, "Deployment and Trajectory Optimization of UAVs: A Quantization Theory Approach," *IEEE Trans. on Wireless Commun.*, vol. 17, pp. 8531–8546, Dec. 2018
- [6] J. Guo and H. Jafarkhani, "Movement-efficient sensor deployment in wireless sensor networks with limited communication range," *IEEE Transactions on Wireless Communications*, vol. 18, pp. 3469–3484, July 2019
- [7] M. Alzenad, A. El-Keyi, F. Lagum, and H. Yanikomeroglu, "3-D Placement of an Unmanned Aerial Vehicle Base Station (UAV-BS) for Energy-Efficient Maximal Coverage," *IEEE Wireless Commun. Lett.*, vol. 6, pp. 434–437, Aug. 2017.
- [8] C. Diaz-Vilor, A. Lozano, and H. Jafarkhani, "Cell-free uav networks: Asymptotic analysis and deployment optimization," *IEEE Trans. on Wireless Commun.*, vol. 22, pp. 3055–3070, May 2023.
- [9] C. Diaz-Vilor, A. Lozano, and H. Jafarkhani, "On the deployment problem in Cell-Free UAV networks," in 2021 IEEE Global Commun. Conf., Dec. 2021.
- [10] C. Diaz-Vilor and H. Jafarkhani, "Optimal 3D-UAV Trajectory and Resource Allocation of DL UAV-GE Links with Directional Antennas," 2020 IEEE Global Commun. Conf., pp. 1–6, Dec. 2020.
- [11] Y. Zeng, X. Xu, and R. Zhang, "Trajectory Design for Completion Time Minimization in UAV-Enabled Multicasting," *IEEE Trans. Wireless Commun.*, vol. 17, pp. 2233–2246, Apr. 2018.
- [12] Q. Wu, Y. Zeng, and R. Zhang, "Joint Trajectory and Communication Design for Multi-UAV Enabled Wireless Networks," *IEEE Trans. Wireless Commun.*, vol. 17, pp. 2109–2121, Mar. 2018.
- [13] J. Guo and H. Jafarkhani, "Sensor Deployment with Limited Communication Range in Homogeneous and Heterogeneous Wireless Sensor Networks," *IEEE Trans. on Wireless Commun.*, vol. 15, pp. 6771–6784, Jul. 2016.
- [14] G. Zhang, H. Yan, Y. Zeng, M. Cui, and Y. Liu, "Trajectory Optimization and Power Allocation for Multi-Hop UAV Relaying Communications," *IEEE Access*, vol. 6, pp. 48566–48576, Aug. 2018.
- [15] S. Zhang, H. Zhang, Q. He, K. Bian, and L. Song, "Joint Trajectory and Power Optimization for UAV Relay Networks," *IEEE Commun. Lett.*, vol. 22, pp. 161–164, Jan. 2018.
- [16] C. You and R. Zhang, "3D Trajectory Optimization in Rician Fading for UAV-Enabled Data Harvesting," *IEEE Trans. Wireless Commun.*, vol. 18, pp. 3192–3207, Jun. 2019.

- [17] J. Guo, E. Koyuncu, and H. Jafarkhani, "A Source Coding Perspective on Node Deployment in Two-Tier Networks," *IEEE Trans. Commun.*, vol. 66, pp. 3035–3049, Jul. 2018.
- [18] S. Karimi-Bidhendi, J. Guo, and H. Jafarkhani, "Energy-efficient node deployment in heterogeneous two-tier wireless sensor networks with limited communication range," *IEEE Trans. on Wireless Commun.*, vol. 20, no. 1, pp. 40–55, 2021.
- [19] F. Cheng, S. Zhang, Z. Li, Y. Chen, N. Zhao, F. R. Yu, and V. C. Leung, "UAV Trajectory Optimization for Data Offloading at the Edge of Multiple Cells," *IEEE Trans. Vehicular Technology*, vol. 67, pp. 6732–6736, Jul. 2018.
- [20] Y. Zeng and R. Zhang, "Energy-Efficient UAV Communication with Trajectory Optimization," *IEEE Trans. Wireless Commun.*, vol. 16, pp. 3747–3760, Jun. 2017.
- [21] Y. Zeng, J. Xu, and R. Zhang, "Energy Minimization for Wireless Communication with Rotary-Wing UAV," *IEEE Trans. Wireless Commun.*, vol. 18, pp. 2329–2345, Apr. 2019.
- [22] Z. Na, C. Ji, B. Lin, and N. Zhang, "Joint Optimization of Trajectory and Resource Allocation in Secure UAV Relaying Communications for Internet of Things," *IEEE IoT Journal*, vol. 9, pp. 16284–16296, Feb. 2022.
- [23] Z. Wang, R. Liu, Q. Liu, J. S. Thompson, and M. Kadoch, "Energy-Efficient Data Collection and Device Positioning in UAV-Assisted IoT," *IEEE IoT Journal*, vol. 7, pp. 1122–1139, Nov. 2020.
- [24] T. Liu, G. Zhang, M. Cui, C. You, Q. Wu, S. Ma, and W. Chen, "Task Completion Time Minimization for UAV-Enabled Data Collection in Rician Fading Channels," *IEEE IoT Journal*, vol. 10, no. 2, pp. 1134– 1148, 2023
- [25] C. Zhan and Y. Zeng, "Completion Time Minimization for Multi-UAV-Enabled Data Collection," *IEEE Trans. on Wireless Commun.*, vol. 18, pp. 4859–4872, Jul. 2019.
- [26] J. Hu, H. Zhang, and L. Song, "Reinforcement Learning for Decentralized Trajectory Design in Cellular UAV Networks With Sense-and-Send Protocol," *IEEE IoT Journal*, vol. 6, pp. 6177–6189, Aug. 2019.
- [27] S. Zhang, H. Zhang, B. Di, and L. Song, "Cellular Cooperative Unmanned Aerial Vehicle Networks with Sense-and-Send Protocol," *IEEE Internet of Things Journal*, vol. 6, pp. 1754–1767, Oct. 2018.
- [28] J. Hu, H. Zhang, L. Song, Z. Han, and H. V. Poor, "Reinforcement Learning for a Cellular Internet of UAVs: Protocol Design, Trajectory Control, and Resource Management," *IEEE Wireless Commun.*, vol. 27, pp. 116–123, Feb. 2020.
- [29] S. Zhang, H. Zhang, Z. Han, H. V. Poor, and L. Song, "Age of Information in a Cellular Internet of UAVs: Sensing and Communication Trade-Off Design," *IEEE Trans. on Wireless Commun.*, vol. 19, pp. 6578–6592, Jun. 2020.
- [30] Y. Yang, Z. Zheng, K. Bian, L. Song, and Z. Han, "Real-Time Profiling of Fine-Grained Air Quality Index Distribution Using UAV Sensing," *IEEE Internet of Things Journal*, vol. 5, pp. 186–198, Nov. 2018.
- [31] T. Kersnovski, F. Gonzalez, and K. Morton, "A UAV system for autonomous target detection and gas sensing," in 2017 IEEE Aerospace Conf., pp. 1–12, Jun. 2017.
- [32] L. Yu, N. Wang, and X. Meng, "Real-time forest fire detection with wireless sensor networks," in *Proc. 2005 Intl Conf. on Wireless Commun., Networking and Mobile Computing*, 2005., vol. 2, pp. 1214–1217, Dec. 2005.

- [33] A. Hossain, P. K. Biswas, and S. Chakrabarti, "Sensing Models and Its Impact on Network Coverage in Wireless Sensor Network," in 2008 IEEE Region 10 and the 3rd. Int. Conf. on Industrial and Information Systems, pp. 1–5, 2008.
- [34] Y. Zou and K. Chakrabarty, "A distributed coverage- and connectivity-centric technique for selecting active nodes in wireless sensor networks," *IEEE Trans. on Computers*, vol. 54, pp. 978–991, Jun. 2005.
- [35] A. Chakraborty, R. R. Rout, A. Chakrabarti, and S. K. Ghosh, "On Network Lifetime Expectancy With Realistic Sensing and Traffic Generation Model in Wireless Sensor Networks," *IEEE Sensors Journal*, vol. 13, pp. 2771–2779, Jul. 2013.
- [36] A. A. Khuwaja, Y. Chen, N. Zhao, M. S. Alouini, and P. Dobbins, "A Survey of Channel Modeling for UAV Communications," *IEEE Commun. Surveys and Tutorials*, vol. 20, pp. 2804–2821, Oct. 2018.
- [37] S. Shimamoto and Iskandar, "Channel characterization and performance evaluation of mobile communication employing stratospheric platforms," *IEICE Trans. Commun.*, vol. E89-B, pp. 937–944, Mar. 2006.
- [38] A. A. Khuwaja, Y. Chen, N. Zhao, M. Alouini, and P. Dobbins, "A Survey of Channel Modeling for UAV Communications," *IEEE Commun. Surveys Tutorials*, vol. 20, pp. 2804–2821, Apr. 2018.
- [39] J. Kazemitabar and H. Jafarkhani, "Multiuser Interference Cancellation and Detection for Users with More Than Two Transmit Antennas," *IEEE Trans. Commun.*, vol. 56, pp. 574–583, Apr. 2008.
- [40] J. Kazemitabar and H. Jafarkhani, "Performance Analysis of Multiple Antenna Multi-user Detection," in *Inf. Theory and Applications Work-shop*, pp. 150–159, Jan. 2009.
- [41] E. Koyuncu and H. Jafarkhani, "Distributed Beamforming in Wireless Multiuser Relay-Interference Networks With Quantized Feedback," IEEE Trans. Inf. Theory, vol. 58, pp. 4538–4576, Jul. 2012.
- [42] A. Adhikary, A. Ashikhmin, and T. L. Marzetta, "Uplink Interference Reduction in Large-Scale Antenna Systems," *IEEE Trans. on Commun.*, vol. 65, pp. 2194–2206, Jan. 2017.
- [43] W. Mei, Q. Wu, and R. Zhang, "Cellular-Connected UAV: Uplink Association, Power Control and Interference Coordination," *IEEE Trans. Wireless Commun.*, vol. 18, pp. 5380–5393, Nov. 2019.
- [44] W. Mei and R. Zhang, "Uplink Cooperative NOMA for Cellular-Connected UAV," *IEEE Journal of Sel. Topics in Sig. Proc.*, vol. 13, pp. 644–656, Feb. 2019.
- [45] Z. Luo and P. Tseng, "On the convergence of the coordinate descent method for convex differentiable minimization," *J. of Optimization Theory and Applications*, vol. 72, pp. 7–35, Jan. 1992.
- [46] M. Diehl, F. Glineur, E. Jarlebring, and W. Michiels, Recent Advances in Optimization and its Applications in Engineering. Springer Berlin Heidelberg, 2010.
- [47] R. W. Heath Jr. and A. Lozano, Foundations of MIMO communication. Cambridge University Press, 2019.
- [48] H. Yousefi'zadeh, H. Jafarkhani, and M. Moshfeghi, "Power optimization of wireless media systems with space-time block codes," *IEEE Trans. on Image Proc.*, vol. 13, pp. 873–884, Jun 2004.
- [49] W. Liu et al., "Energy harvesting wireless sensor networks: Delay analysis considering energy costs of sensing and transmission," *IEEE Trans. on Wireless Commun*, vol. 15, pp. 4635–4650, Mar. 2016.
- [50] Z. Sheng, C. Mahapatra, V. C. Leung, M. Chen, and P. K. Sahu, "Energy efficient cooperative computing in mobile wireless sensor networks," *IEEE Trans. on Cloud Computing*, vol. 6, pp. 114–126, Jul. 2015.
- [51] R. Ding, F. Gao, and X. S. Shen, "3D UAV Trajectory Design and Frequency Band Allocation for Energy-Efficient and Fair Communication: A Deep Reinforcement Learning Approach," *IEEE Trans. on Wireless Commun.*, vol. 19, pp. 7796–7809, Aug. 2020.
- [52] J. E. Mitchell, "Branch-and-cut algorithms for combinatorial optimization problems," *Handbook of applied optimization*, vol. 1, no. 1, pp. 65– 77, 2002.
- [53] S. P. Boyd and L. Vandenberghe, Convex optimization. Cambridge University Press, 2004.
- [54] M. Hua, L. Yang, Q. Wu, and A. L. Swindlehurst, "3D UAV Trajectory and Communication Design for Simultaneous Uplink and Downlink Transmission," *IEEE Trans. on Commun.*, vol. 68, pp. 5908–5923, Jun. 2020.